Ammonium Recruitment and Ammonia Transport by *E. coli* Ammonia Channel AmtB

Thomas P. Nygaard,* Carme Rovira,† Günther H. Peters,* and Morten Ø. Jensen‡
*MEMPHYS - Center for Biomembrane Physics, Department of Chemistry, Technical University of Denmark, Lyngby, Denmark;
†Centre de Recerca en Química Teòrica, Barcelona, Spain; and ‡Department of Life Sciences and Chemistry, Roskilde University, Roskilde, Denmark

ABSTRACT To investigate substrate recruitment and transport across the *Escherichia coli* Ammonia transporter B (AmtB) protein, we performed molecular dynamics simulations of the AmtB trimer. We have identified residues important in recruitment of ammonium and intraluminal binding sites selective of ammonium, which provide a means of cation selectivity. Our results indicate that A162 guides translocation of an extraluminal ammonium into the pore lumen. We propose a mechanism for transporting the intraluminally recruited proton back to periplasm. Our mechanism conforms to net transport of ammonia and can explain why ammonia conduction is lost upon mutation of the conserved residue D160. We unify previous suggestions of D160 having either a structural or an ammonium binding function. Finally, our simulations show that the channel lumen is hydrated from the cytoplasmic side via the formation of single file water, while the F107/F215 stack at the inner-most part of the periplasmic vestibule constitutes a hydrophobic filter preventing AmtB from conducting water.

INTRODUCTION

Ammonia/ammonium (Amm) is an essential growth factor in bacteria, yeasts, plants, and fungi, while it is toxic to mammalian cells. Proteins belonging to the ammonia transporter family have been identified in a wide range of organisms; ammonia transporter (Amt) proteins in bacteria and plants, methylammonium/ammonium permeases in yeasts, and Rhesus blood-group associated glycoproteins in animals (1,2). Certain Amt proteins are, in addition, capable of transporting methylammonium (MeAmm) (3–7), while some Rhesus proteins also can transport CO_2 (8).

The first Amt protein for which high resolution crystallographic structures have been solved is *Escherichia coli* Ammonia transporter B (AmtB) (9,10). In one study, three sequentially identical mutated structures were reported (9). We refer to these as the Khademi structures. A second study reported two wild-type (wt) structures (10). We refer to these as the Zheng structures.

As shown in Fig. 1 *A*, three identical AmtB monomers form a trimer (9–12). The AmtB monomer has 11 transmembrane-spanning α-helices (TM1–TM11) arranged in a right-handed bundle (Fig. 1 *A*). Depressions in both the periplasmic and the cytoplasmic surfaces (vestibules) lead into a hydrophobic pore lined by Histidines H168 and H318 (Figs. 1 *B* and 4 *A*), which, by sharing an H-atom between their imidazole rings, are mutually fixed (9,10). Aromatic residues F103, F107, and W148, together with the hydrogen acceptor S219:O_γ, have been suggested to define a substrate binding site for $NH_4^+/MeNH_3^+$ at the periplasmic pore entrance (9,10,13).

The Khademi structure (Protein DataBank (PDB) entry No. 1U7G) is so far the only x-ray structure where Amm molecules are proposed to occupy the channel, i.e., by one extraluminal NH_4^+ and three intraluminal gaseous NH_3 (9). This is in accordance with experimental AmtB data, which consistently indicate gradient-driven NH_3 uniport, i.e., diffusion or passive transport (6,9,14). However, controversy about which Amm species are recognized by AmtB prevails. The most common view is NH_4^+ recognition (9,10,14), but NH_3 recognition has also been proposed (6).

Noteworthy is that the NH_3 diffusion across AmtB is similar to that across bilayers (9). This questions the biological significance of AmtB, albeit enhanced recruitment of Amm, i.e., NH_4^+, could be one justification. Amm transport mechanisms based on *E. coli* AmtB have been proposed (9,10). However, the detailed mechanism of NH_4^+ recruitment and NH_3 conduction, and their relationships to the structure of AmtB are unknown at the molecular level (10). To gain such insight, we conducted classical mechanical molecular dynamics (MD) simulations of AmtB.

MATERIALS AND METHODS

This section provides information about the simulation setup, chosen parameters, simulation details, and pK_a calculations.

System setup

The crystal structure of monomeric AmtB with the mutations F68S, S126P, and K255L, and all Methionines replaced by Selenomethionine (Mse) was obtained from the PDB as No. 1U7G (9). We chose this crystal structure because Amm presumably occupies the substrate binding site and the channel lumen and because the two Zheng structures lack coordinates for residues in loops connecting helix TM5 to TM6 and TM9 to TM10 (10).

Submitted May 22, 2006, and accepted for publication September 7, 2006.

Address reprint requests to Morten Ø. Jensen, D. E. Shaw Research, New York, NY 10036. E-mail: morten.jensen@deshaw.com.

0006-3495/06/12/4401/12 $2.00

doi: 10.1529/biophysj.106.089714

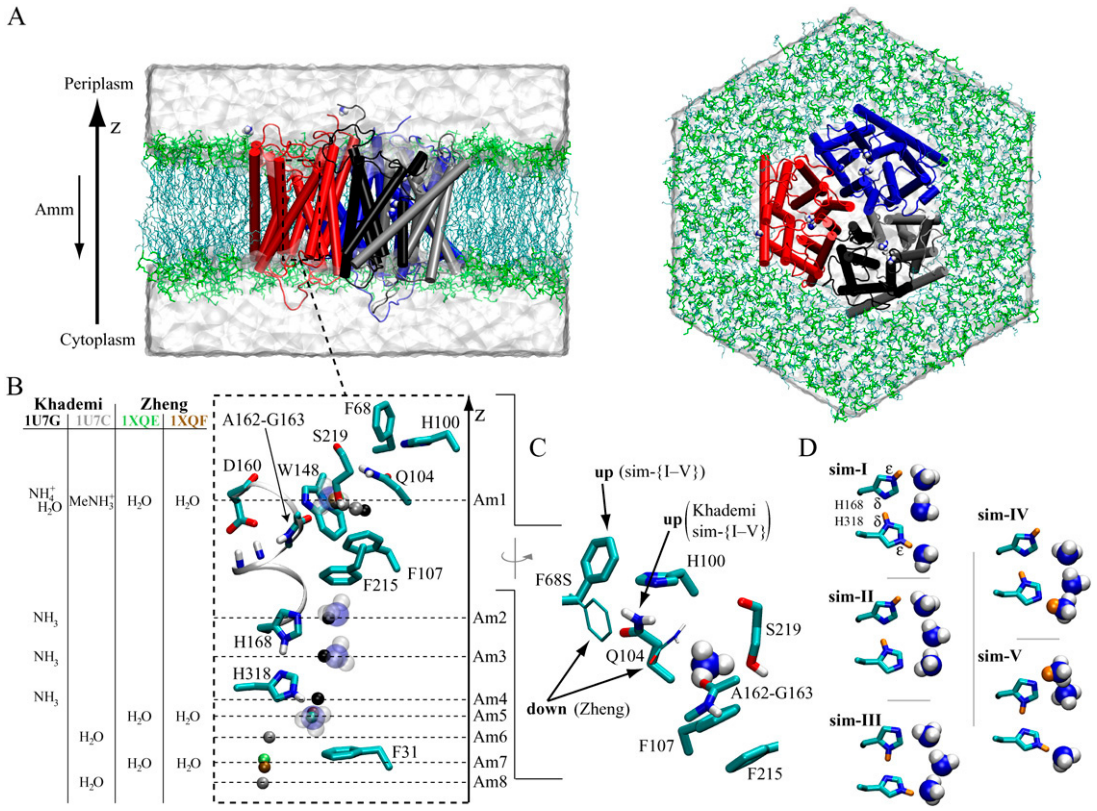

FIGURE 1 The simulated system. (*A*) Snapshot of sim-III (see Table 1) showing side and top views of the AmtB trimer with monomers colored red, blue, and gray/black, respectively. Lipid headgroups and hydrophobic tails are colored green and cyan, respectively. Water is depicted in transparent surface representation, and Amm molecules appear in blue and white vdW representation. The quasi twofold symmetry-related helices of one of the monomers are colored gray and black. The physiological direction of Amm transport in *E. coli* is indicated. (*B*) Enlargement of key residues of the substrate binding site, F68, H100, Q104, F107, W148, D160, A162-G163, and S219; and of the pore lumen, F31, H168, F215, and H318 (note the helix-stabilizing function of D160). The corresponding simulation snapshot of NH_3 and NH_4^+ is depicted as transparent vdW spheres. Solid spheres represent selected water molecules, Amm, or MeAmm molecules in the crystal structures of AmtB as tabulated, and their positions are numbered Am1–Am8 (an extension of the numbering scheme used by Khademi et al. (9)). Substrates of the Khademi structures are colored black (1U7G) and gray (1U7C) (9), while those of the Zheng structures are colored green (1XQE) and brown (1XQF) (10). The positions of water in the third reported Khademi structure (1U77) match closely those found in 1U7C and 1U7G, and were not included in the representation. (*C*) Key configurational deviations of the substrate binding site. The Zheng down-configurations of Q104 and F68 (*thin licorice*) are depicted along with the corresponding Khademi up-configuration of Q104. The S68 residue in the Khademi structures is not shown; instead, the F68 up-configuration adopted in the starting structures for our initial simulations is depicted (see Table 1). (*D*) Assigned protonation states of H168, H318, and Amm adopted in our simulations. For sim-I the δ- and ϵ-nitrogens of H168 and H318 are labeled. The differently placed protons are colored orange. The snapshots are of energy-minimized systems from which our simulations were started. For easing visual comprehension, figures showing explicit residues in the protein structure are all viewed from the same angle as chosen for Fig. 1 *B*. Exceptions are Fig. 1 *C* and Fig. 3, *B* and *C*, which are rotated around the *z* axis.

Double side-chain coordinates (A and B) existed for residues Mse{200,328}, I15, S{43,155,335,358}, V{60,281,308}, L{88,259}, T203, and C326 (9). We used the A-coordinates. All introduced mutations were backmutated to the appropriate wt residues. Due to the F68S mutation in the Khademi structures, Q104 takes a different configuration (up) than in the Zheng structures (down), as shown in Fig. 1 *C*. All other residues defining the substrate-binding site are identically positioned in all five *E. coli* AmtB crystal structures (9,10). For sim-{I–V} we adopted the up-configuration of Q104 from the Khademi structure 1U7G, which differs from the Zheng down-configuration by a rotation of the C_α-C_β-C_γ-C_δ dihedral. Due to steric hindrance of Q104 we placed the backmutated F68 side chain in an up-configuration above the neighboring H100 imidazole ring (Fig. 1 *C*).

Conventional (pH = 7) protonation states were chosen for all Aspartatic and Glutamic acids and for Lysine residues. Based on visual inspection, N_ϵ protonation was chosen for all Histidine residues except for luminal H168 and H318. These two adjacent Histidines are positioned such that a proton is shared between their N_δ atoms. For classical mechanical MD simulations in explicit water the proton has to be permanently assigned to one of the two Histidines. We assigned protons to these Histidines in three different ways, as shown in Fig. 1 *D* (see also Table 1). For the charged state in sim-I, we determined to which N_δ atom of H168 and H318 the shared proton is most likely bound by estimating their pK_a values (see pK_a Calculations). Since protonation of H318:N_δ is favored over protonation of H168:N_δ, H318:N_δ was protonated in sim-I.

Hydrogen atoms were added to the monomer and crystal waters using PSFGEN distributed with NAMD (15). The trimeric structure of AmtB was generated with VMD (16) using the transformation matrices provided in the PDB file. The symmetry related atoms 549, 678, and 767, all being oxygen atoms of water molecules, were not included in the transformation, but were added after the trimer was constructed. Cysteines C109 and C56 are close enough to form a disulfide bond, but the electron density map (9) does not show evidence of such a bond and it was therefore not introduced.

For the lipid membrane, POPE lipids (16:0/18:1c9) were used. This lipid resembles well the PE rich *E. coli* membrane (17). In accordance with the experimental value for lamellar phase (18), a bilayer with 40 Å vertical separation between phosphorous headgroup atoms was constructed from 1920

cis-POPE lipids arranged in a regular hexagonal lattice with a lattice vector of 8.3 Å. The membrane plane was chosen parallel to the *x*,*y* plane. When positioning AmtB into the membrane, lipids overlaying or within 2 Å of the AmtB trimer (including crystal water) were deleted. An identical number of lipids were retained in the upper and lower leaflet. Crystal waters within the hydrophobic part of the bilayer (-15 Å $\leq z$ or $z \geq 15$ Å) but outside the protein interior were removed. SOLVATE (19) was subsequently used to add an ellipsoidal solvation shell around the membrane and the solvent-exposed parts of AmtB.

Given the trimeric structure of AmtB it is feasible to use a hexagonal simulation cell. A hexagonal periodic box was cut out in the *x*,*y* plane from the above system, while ensuring a minimum distance of 30 Å between the protein complex and the edges of the hexagonal box. The resulting hexagonal basis vectors (in Å) were $\mathbf{v}_1 = (141.1, 0.0, 0.0)$, $\mathbf{v}_2 = (70.6, 122.2, 0.0)$, and $\mathbf{v}_3 = (0.0, 0.0, 84.0)$. The corresponding dimensions of the AmtB trimer were 73.6 Å in the $\mathbf{v}_1$ and $\mathbf{v}_2$ directions, and 66.9 Å in the $\mathbf{v}_3$ direction. An appropriate number of water molecules were replaced by chloride counterions to bring the system to overall neutrality. The final system for sim-I consisted of an AmtB trimer (17,106 atoms), 9 NH_3 molecules (36 atoms), 3 NH_4^+ ions (15 atoms), 400 POPE lipids (50,000 atoms), 25,029 water molecules (75,087 atoms), and 12 Cl^- ions (12 atoms), adding up to a total system size of 142,256 atoms. When changing the protonation states of H168, H318, and NH_3 molecules (to NH_4^+), the number of counterions were adjusted accordingly.

Parameters

We used the CHARMM 27 parameter set (20). The CHARMM neutral aliphatic amines parameters (21) were used for NH_3 molecules. No CHARMM parameters are available for NH_4^+ ions, but identical Lennard-Jones parameters are used for all nitrogen atom types in the CHARMM 27 parameter set, albeit different from those developed for NH_3 (21). To be consistent with the existing force field, we decided to use the CHARMM 27 parameters of the ammonium nitrogen. Bond and bond-angle parameters were chosen to be the same as for the $-NH_3^+$ moiety of Lysine. For partial charges of NH_4^+, OPLS charges are available (22). OPLS charges are as CHARMM charges optimized to reproduce experimental data. OPLS and CHARMM partial charges of $-NH_3^+$ in Lysine are nearly identical (20,22). Therefore we found it appropriate to use the OPLS partial charges for NH_4^+.

Simulation details

Molecular dynamics simulations were conducted using NAMD (15). Temperature and pressure were controlled by a Langevin thermostat and barostat, respectively. The integration time step was 1 fs and coordinates were saved every 0.5 ps. Electrostatic interactions were treated using the particle-mesh Ewald method, with a grid spacing <1.0 Å, using a multiple timestepping scheme. The van der Waals interactions were cut off at 12 Å using a switching function starting at 10 Å. Full periodic boundary conditions were imposed.

Initially, the systems were minimized while keeping protein, Amm, and crystal water fixed. An additional minimization without fixation was subsequently performed. The systems were then equilibrated for 250 ps while fixing the above-mentioned parts. After equilibration, the systems were again minimized without fixation. MD simulations without fixation were then performed for at least 2 ns at $T = 310$ K and $P = 1$ atm (NPT ensemble).

pK_a calculations

When appropriate we carried out electrostatic pK_a calculations to estimate the pK_a shifts (ΔpK_a) of H168 and H318 to determine their preferred protonation states. In the calculations we included all protein and Amm partial charges. The partial charges were taken from CHARMM 27 and OPLS, respectively. Following the approach of Faraldo-Gomez and Roux (23) we used a water probe of radius 1.4 Å to determine the protein solvent-accessible surface representing the dielectric boundary to the surrounding water and membrane. These were treated implicitly by means of dielectric constants of $80\epsilon_0$ and $2\epsilon_0$, respectively. The membrane was represented by a 40 Å thick slab centered at the geometrical center of the monomer. Due to overlap between the membrane slab and the two water-filled vestibules leading into channel lumen, these were explicitly assigned a dielectric constant of $80\epsilon_0$. In all calculations we used a cubic grid with 1 Å grid spacing and with *x*, *y*, and *z* dimensions being at least twice the AmtB monomer dimensions. This ensured that an applied focusing procedure (same calculation, but with half the grid spacing, and boundary conditions given from the unfocused calculation) encapsulated the entire monomer. Before the calculations, any grid points not assigned above were assigned a dielectric constant of $80\epsilon_0$. The electrostatic potential was obtained by solving the Poisson-Boltzmann equation implemented in CHARMM (24). From this, the ΔpK_a values were derived.

For the intraluminal protonation state of sim-I, we had to determine to which N_δ atom of H168 and H318 in the starting structure the shared proton is most likely bound. For that purpose both Histidines were initially protonated at the N_ϵ position. pK_a shifts were then calculated for protonation at each N_δ and with different dielectric constants assigned to the protein ($\epsilon_p = \{2,4,6,8\}\epsilon_0$). In all cases the largest pK_a shift was obtained for protonation of H318:N_δ ($\Delta pK_a = \{6.7,2.7,1.5,1.0\}$), leading to relative pK_a shifts [ΔpK_a(H318:N_δ)/ΔpK_a(H168:N_δ)] in the range 2.4–3.8.

To identify the preferred neutral protonation state of H168 and H318, we calculated ensemble-averaged $\langle \Delta pK_a(\text{H168:N}_\epsilon) \rangle$ and $\langle \Delta pK_a(\text{H318:N}_\epsilon) \rangle$ values for sim-I, sim-II^{wt}_{noAmm}, and sim-III^{wt}_{noAmm}. In none of the calculations did we include water explicitly. Thereby, ΔpK_a values for a channel devoid of any substrate was obtained for sim-II^{wt}_{noAmm} and sim-III^{wt}_{noAmm}. For all simulations in consideration, $\langle \Delta pK_a(\text{H168:N}_\epsilon) \rangle$ and $\langle \Delta pK_a(\text{H318:N}_\epsilon) \rangle$ were calculated by changing the given intraluminal protonation state to that of sim-III and sim-II, respectively, and subsequently protonating either H168:N_ϵ or H318:N_ϵ. For these calculations a dielectric constant of $\epsilon_p = 2\epsilon_0$ was assigned to the protein. When no Amm is present in the lumen (sim-II^{wt}_{noAmm}, sim-III^{wt}_{noAmm}), $\langle \Delta pK_a(\text{H168:N}_\epsilon) \rangle$ is relatively larger than $\langle \Delta pK_a(\text{H318:N}_\epsilon) \rangle$, due to a stabilization of H168:N_ϵH by T273:O_γ. This is compensated when intraluminal Amm is present (sim-I), which then yields $\langle \Delta pK_a(\text{H318:N}_\epsilon) \rangle$ larger than $\langle \Delta pK_a(\text{H168:N}_\epsilon) \rangle$.

RESULTS AND DISCUSSION

In our simulations we initially considered five different intraluminal protonation states as shown in Fig. 1 *D* and as summarized in Table 1. We use the term ''intraluminal protonation state'' for the combined protonation states of H168, H318, and intraluminal Amm. We correspondingly refer to these simulations as sim-I, sim-II, sim-III, sim-IV, and sim-V, or sim-{I–V}. In all five simulations one NH_4^+ is positioned extraluminally at the substrate binding site. In sim-I a positive charge is localized at H318. The simulations sim-II and sim-III are both of neutral tautomeric H168 and H318 protonation states. The simulations sim-IV and sim-V correspond to sim-II and sim-III but with one intraluminal NH_3 substituted by NH_4^+. We also conducted simulations of intraluminal protonation states identical to sim-II and sim-III, but with changes in the protein structure at the periplasmic NH_4^+ binding site (superscript *wt*), with protonated H100 (subscript $H100^+$), and with the channel devoid of Amm (subscript *noAmm*).

In the following, we discuss 1), recruitment and binding of NH_4^+ to the substrate binding site; 2), NH_4^+ transfer from the substrate binding site to pore lumen; 3), intraluminal Amm

TABLE 1 Summary of the simulations

	Lumen		Substrate				Substrate binding site				
Simulation	[H168:N_ϵ	H318:N_ϵ]	[Am1	Am2	Am3	Am4]	[F68	Q104	H100:N_ϵ]	Amm constrained	Length (ns)
sim-I	H	H (+)	NH_4^+	NH_3	NH_3	NH_3	up	up	H	no	2.2
sim-II	H		NH_4^+	NH_3	NH_3	NH_3	up	up	H	no	1.9
sim-III		H	NH_4^+	NH_3	NH_3	NH_3	up	up	H	no	3.0
sim-IV	H		NH_4^+	NH_3	NH_3	NH_4^+	up	up	H	no	2.0
sim-V		H	NH_4^+	NH_4^+	NH_3	NH_3	up	up	H	no	1.9
sim-III^{wt}_{fix}		H	NH_4^+	NH_3	NH_3	NH_3	down	down	H	yes	2.0
sim-III^{wt}		H	NH_4^+	NH_3	NH_3	NH_3	down	down	H	no*	4.0
sim-$III^{wt}_{H100^+}$		H	NH_4^+	NH_3	NH_3	NH_3	down	down	H (+)	no*	4.0
sim-II^{wt}_{noAmm}	H		—	—	—	—	down	down	H	—	10.0
sim-III^{wt}_{noAmm}		H	—	—	—	—	down	down	H	—	10.0

The lumen, substrate, and substrate binding site configuration of each simulation and applied constraints and simulation lengths. *H* indicates N_ϵ-protonation of Histidines H100, H168, and H318, while blank (no *H*) indicates N_δ-protonation. The +-symbol indicates positively charged Histidines with both imidazole nitrogens protonated. Am1–Am4 are substrate locations in the Khademi structure 1U7G (9). The terms ''up'' and ''down'' denote distorted and wt configurations, respectively, of the substrate binding site residues F68 and Q104 (see text). ''Constrained'' implies that Amm molecules are fixed at the substrate locations in the x-ray structure.

*Restarted from sim-III^{wt}_{fix} with Amm released.

dynamics; 4), Amm exit to cytoplasm; and 5), channel hydration. Finally we propose a plausible mechanism integrating NH_4^+ recruitment and translocation to pore lumen, and the backward relay of the intraluminally recruited proton to the periplasm leading to net transport of NH_3 only.

Interactions at the substrate binding site

Trajectories (*z*-coordinates) of the extraluminal NH_4^+ and of the three intraluminal Amm are shown for sim-{I–V} in Fig. 2. Surprisingly, the NH_4^+ ion initially located at the Am1 position and partially coordinated to water was generally found to leave this position. To elucidate if this observation was biased by our starting conditions, we initially constrained NH_4^+ to the Am1 position for 2 ns, which, however, led to the same result (sim-III^{wt}_{fix}, Table 1, data not shown). The escape of NH_4^+ from the substrate binding site could be due to shortcomings of the used force field, i.e., a possible poor description of cation-π interactions between NH_4^+ and aromatic residues at the substrate-binding site. These are only implicitly accounted for by the nonbonded interaction terms in the CHARMM energy function. Cation-π interactions can be treated explicitly by using polarizable force fields or ab initio methods. We have conducted ab initio calculations of the substrate binding site based on structures generated from ab initio MD (Carr-Parinello MD) simulations of AmtB. Our results indicate that cation-π interactions are not the main contribution to the binding of NH_4^+ (data not shown). Thus, we do not expect that the easy escape of NH_4^+ should be assigned as a shortcoming of the force field, rather it should be interpreted as an effect of the substrate binding site being a low-affinity cation binding site. When close to the Am1 position, we observe that NH_4^+ is involved in one or more prominent hydrogen-bond (H-bond) interactions with F161:O, A162:O, W148:N_ϵ, D160:O_δ, D160:O, S219:O, and S219:O_γ, as shown in the histogram of NH_4^+-protein interactions in Fig. 3 *A*. These interactions reflect NH_4^+-protein interactions at positions slightly displaced from the Am1 position as shown in Fig. 3 *B*. Most interesting is the interaction with A162:O, which we will refer to as A162:C=O or as A162-G163 when referring to the entire peptide bond. In the crystal structures, A162:C=O points in-between the π-stacking side chains of F107 and F215 (Fig. 3 *C*, *inset*). In our simulations, A162:C=O reorients to point either into the substrate binding site (up) or into the pore lumen (down) (Fig. 3 *C*). The role of A162-G163 is further discussed below. Also interesting is the interaction between NH_4^+ and D160. Upon rotation of the carboxylate group, D160 becomes a hydrogen acceptor to NH_4^+ (Fig. 3 *B*), while it still retains one of its two H-bonds that fix the irregular helical structure at the periplasmic constriction region (Fig. 1 *B*). The mutation D160A inactivates AmtB, suggesting that D160 is involved in Amm binding and/or transport (25). The role of D160 has also been proposed to be structural in fixing surrounding residues (9,10). Our simulations support both views, i.e., that D160 participates in ordering the surrounding protein structure, and, in recruiting and binding of Amm, first via its carbonyl oxygen and subsequently via its carboxylate group.

Q104 influence on substrate binding site occupation

Simulations sim-{I–V} generally show rapid escape of extraluminal NH_4^+ (Fig. 2) and slow relaxation of F68 and Q104 toward their wt down-configurations (Fig. 1 *C*). It is therefore of interest to examine whether or not F68 and Q104 influence substrate recruitment and occupation of the substrate binding site, since the functional importance of this recruitment site has remained unclear (9,10,13). Accordingly, we changed the configurations of F68 and Q104 in the Khademi

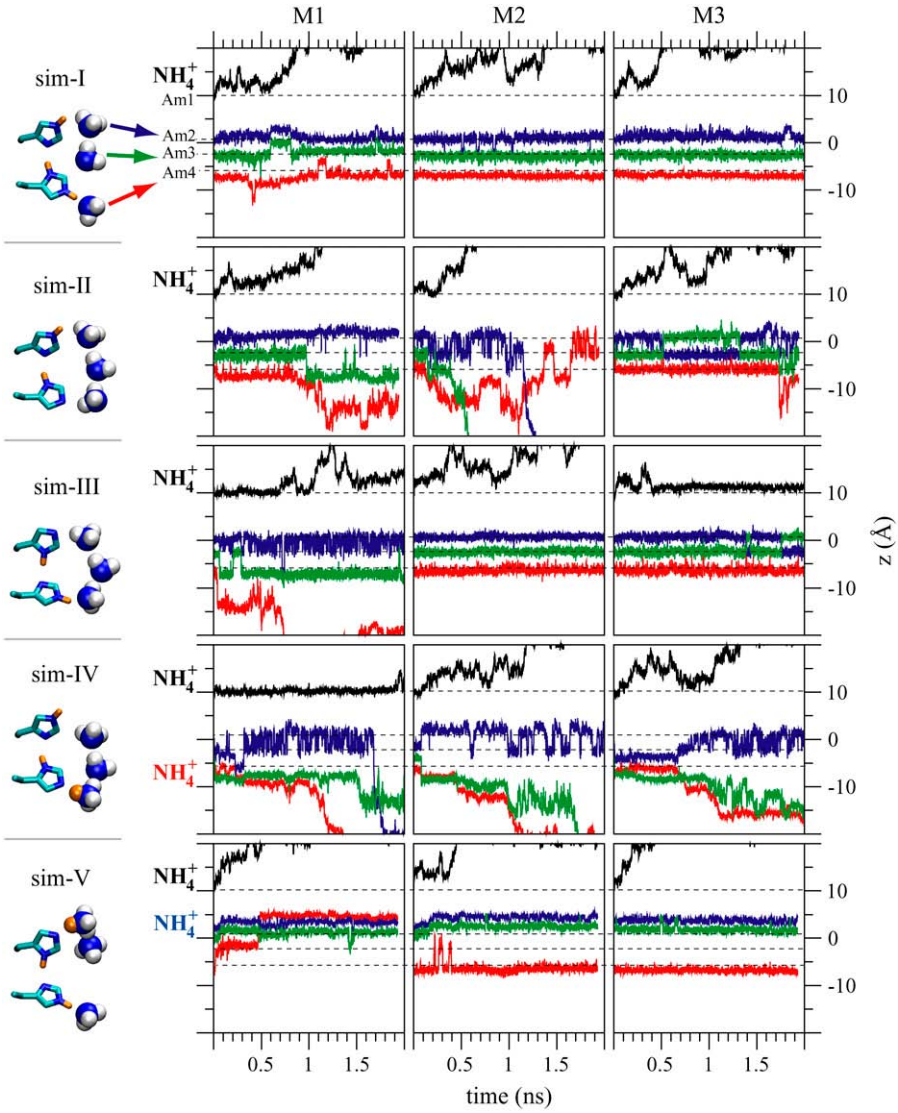

FIGURE 2 Trajectories. Amm z-coordinates as function of time for simulations sim-{I–V}. (*Black*) NH_4^+ initially at the Am1 position. (*Blue*) NH_3/NH_4^+ initially at the Am2 position. (*Green*) NH_3 initially at the Am3 position. (*Red*) NH_3/NH_4^+ initially at the Am4 position. M1, M2, and M3 refer to the individual monomers in the AmtB trimer. The Am1–Am4 positions are indicated by dashed lines. The strongest correlation between Amm molecules is observed between NH_4^+ and NH_3, e.g., red and green curves in sim-IV, and blue and green/red curves in sim-V. Occasionally, some correlation is observed between the two NH_3 closest to the periplasm. These may however also interchange positions; see, e.g., blue and green curves of monomer M3 in sim-II and sim-III.

structure 1U7G to the down-configurations as observed in the Zheng structures. We used the same intraluminal protonation state as in sim-III and simulated initially with Amm fixed for 2 ns (sim-III^{wt}_{fix}) and subsequently continued for 4 ns with Amm released and H100 being either neutral (sim-III^{wt}) or protonated (sim-III^{wt+}_{H100}). The solvent-accessible H100, fixed by a hydrogen bond to Y64:H_γ, may be protonated given the pH in *E. coli* periplasm [$pH_{periplasm} < pH_{cytosol} \simeq 7.6$ (26)] and thereby affect the dynamics of neighboring F68 and Q104. However, regardless of the protonation state of H100, none of the above simulations revealed any significant correlation between NH_4^+ occupation of the substrate binding site and the F68/Q104 dynamics.

The F68/Q104 dynamics might be important for recruiting substrates other than NH_4^+, and was therefore further investigated. We find that Q104 adopts several different up-configurations, which are not related to specific H-bond interactions, neither with the substrate nor with the protein, e.g., with H100. These observations in wt AmtB simulations dispute that Q104 up-configurations are solely caused by the F68S mutation (10). Rather, we find that they also may result from steric effects, e.g., the space made available by F68 and H100. Since we do not observe Q104 to affect binding of NH_4^+ we propose that Q104 by means of sterical effects influence the binding of the methyl group in MeAmm. This may explain why Amm is a better AmtB substrate than MeAmm (6,14).

Entry and exit of NH_4^+ at the substrate binding site

When NH_4^+ leaves the substrate binding site we find that it becomes fully hydrated (Fig. 5 *A*) and diffusively migrates out of the periplasmic vestibule within 0.5–1.5 ns (Fig. 2). The calculated diffusion constant is 0.83×10^{-5} cm^2/s, which is equal to that of free diffusion $0.82(\pm 0.02) \times 10^{-5}$ cm^2/s (27). While NH_4^+-protein interactions are specific at the

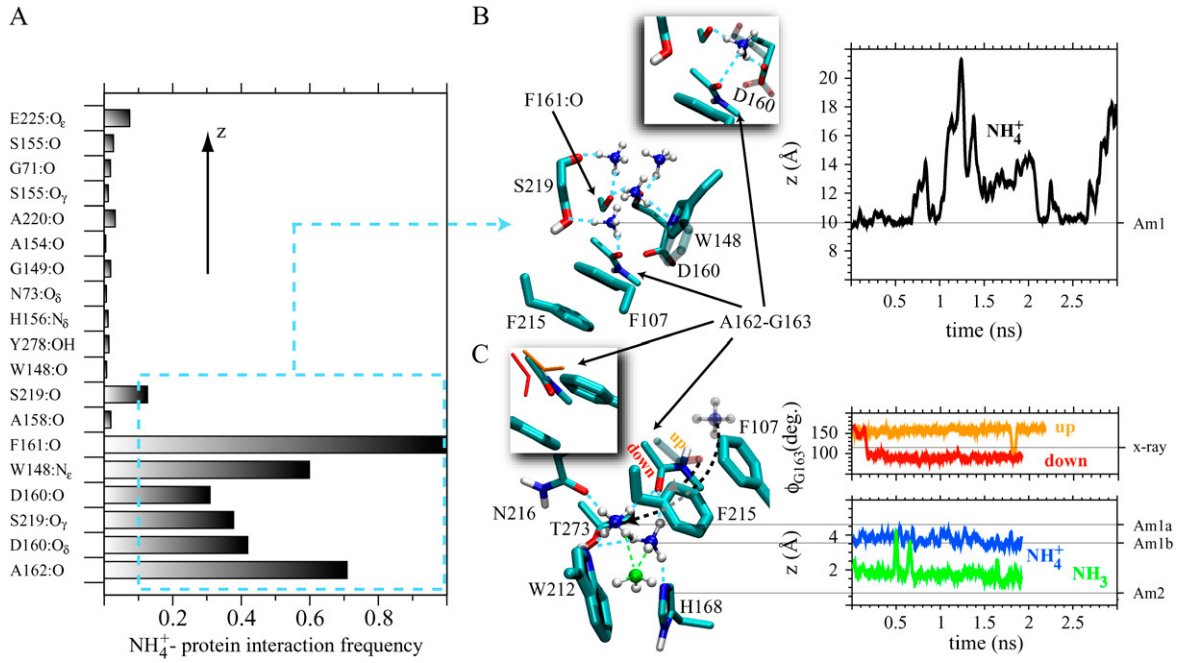

FIGURE 3 NH_4^+ recruitment and translocation. (*A*) Histogram of H-bonding interactions in sim-{I–V} between NH_4^+ and residues in the periplasmic vestibule. The residues are ordered according to their *z*-coordinates. The histogram was constructed by counting the occurrences of NH_4^+ within protein distances below 3 Å and normalizing the maximum count to 1. (*B*) Five snapshots of NH_4^+ (un-)binding at the substrate binding site along the sim-III trajectory. The snapshots are of representative NH_4^+ positions, which cause the most prominent H-bond interactions of the histogram in *A*. The inset shows the binding state where the D160 carboxylate group is rotated to accept an NH_4^+ hydrogen. The right panel shows the trajectory (*z*-coordinate) of NH_4^+ in monomer M1. The snapshots were aligned by minimizing the RMSD between all C_α atoms. (*C*) Two snapshots of NH_4^+ at intraluminal binding sites in the periplasmic constriction region (sim-V). The additional NH_4^+ (*transparent*) corresponds to the bottom position in *B* with A162:C=O in the up-conformation (*transparent*). In the up-configuration A162:C=O can form an H-bond to water if no NH_4^+ is present (not shown). When NH_4^+ is positioned intraluminally A162:C=O reorients to a down-conformation (*solid*). We name the two intraluminal NH_4^+ positions Am1a and Am1b. In the Am1a state NH_4^+ H-bonds to A162:C=O, W212:N_ϵ/T273:O_γ, N216:O_δ, and NH_3. In the Am1b state NH_4^+ H-bonds to A162:C=O, H168:N_ϵ, W212:N_ϵ/T273:O_γ, and NH_3. The NH_4^+ hydrogen coordinating to W212:N_ϵ/T273:O_γ shifts between these two hydrogen acceptors, which are themselves H-bonded via W212:N_ϵH. The black dashed arrow indicates the direction of NH_4^+ translocation across the F107/F215 stack. An opening of the stack can be recognized. The inset shows the x-ray structure position of A162:C=O and the corresponding closed conformation of the F107/F215 stack. The right panels show ϕ_{G163} trajectories of sim-III, monomer M1 (*orange* and mainly ''up'') and sim-V, monomer M3 (*red* and mainly ''down''), and the *z*-coordinates of NH_4^+ (*blue*) and NH_3 (*green*) in sim-V, monomer M3. Note that the viewing angle in *B* and *C* is different from Fig. 1 *B*.

substrate binding site, they are less specific in the periplasmic vestibule. There, we find that NH_4^+ mainly interacts with backbone carbonyl groups (Fig. 3, *A* and *B*). Further out the vestibule a somewhat more specific interaction is again observed; namely with the carboxylate group of E225, which, located within one of four loops surrounding the periplasmic vestibule, protrudes into the solvent. The other three loops have residues E70, E87, and E344 located in similar positions (Fig. 4 *A*), and these four Glutamic acids, which we modeled in their charged form, may therefore be considered as NH_4^+ capturing residues.

A162 guided ammonium translocation

Pore-blocking F107 and F215 have identical π-stacking conformations in all five crystal structures (9,10). Another common feature is that the backbone carbonyl group of the conserved A162 is directed toward the space in-between the F107/F215 stack (Fig. 3 *C*, *inset*).

In our simulations A162:C=O predominantly takes a conformation pointing up toward and into the substrate binding site, forming a H-bond to either extraluminal NH_4^+ or water (Fig. 3 *C*). A striking exception from this observation is sim-V, where we introduced intraluminal NH_4^+, which occupies the intermediate positions Am1a–b between Am1 and Am2 (Fig. 3 *C*). In this case A162:C=O shifts to a down-conformation, thereby forming a H-bond to intraluminal NH_4^+, which in turn is stabilized significantly at this position (Fig. 3 *C*). A162:C=O moves 3–4 Å along *z* when shifting between up- and down-conformations. As depicted in Fig. 3 *C*, the shift is facilitated by the adjacent G163 via a change of its ϕ-torsion from ~160° to ~95°. A162:C=O has been speculated to be a hydrogen acceptor for substrate molecules in a transient open state of the constriction region (10). Based on our two observed conformations we suggest that the function of A162:C=O is to actively guide NH_4^+ across the periplasmic constriction, i.e., across the F107/F215 stack via direct H-bonding interactions.

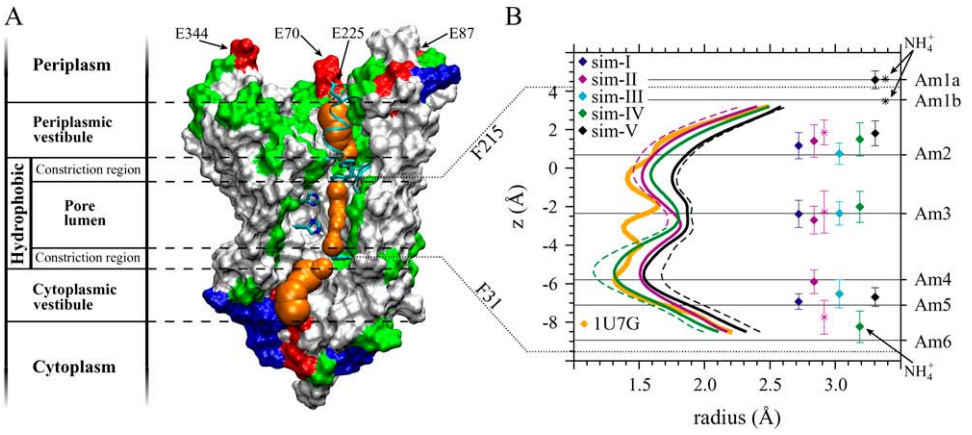

FIGURE 4 Channel characteristics and intraluminal Amm positions. (*A*) Side view of AmtB and definition of channel regions (9,10). The protein is shown in surface representation and colored according to residue types; red is acidic, blue is basic, green is polar, and white is nonpolar. Four Glutamic acids, which surround the periplasmic vestibule and might be important in attracting NH_4^+ to the substrate binding site, are pointed out. Orange spheres represent the pore with their radii calculated using HOLE (28). (*B*) The intraluminal pore radii for the Khademi 1U7G structure (*orange*), and the average pore radii for sim-{I–V} over the last 1 ns of each simulation (also averaged over monomers) are shown. Dashed lines are maximal upper (sim-V) and lower (sim-II and sim-IV) limits of the radii calculated from the respective standard deviations. Average positions of intraluminal Amm are indicated by diamonds and stars. For each of sim-I, sim-III, and sim-IV, only one entry (*diamonds*) is shown representing averages over all three monomers. For sim-II, the diamonds correspond to monomer M3, where all NH_3 are present in the channel lumen, while stars represent an average of M1 and M2 data, where the channel lumen is partially occupied. For sim-{IV,V} intraluminal NH_4^+ positions are pointed out.

Intraluminal NH_4^+ in the upper part of the pore lumen (sim-V) is strongly stabilized by tetrahedral coordination to channel-lining residues. Three of the NH_4^+ hydrogens are coordinated to A162:C=O, W212:N_ϵ/T273:O_γ, and NH_3, respectively, while the remaining hydrogen coordinates either to N216:O_δ or to H168:N_ϵ (Fig. 3 *C*). Given this intraluminal stabilization, in particular at position Am1b, we suggest that NH_4^+ may translocate from the substrate binding site to the Am1b position before deprotonation, rather than to the Am2 position as previously proposed (9). Both scenarios require that H168:N_ϵ is deprotonated, implying that neutral H168:N_δH-H318:N_ϵH (sim-{III,V}, Fig. 1 *D*) is the native protonation state of the intraluminal Histidines before any proton relay involving these residues.

In all our simulations, correlated side-chain rotations of 180° of F107 and F215 are frequently observed, except in sim-V, where the side chains are rotated and rotationally constrained. This results in a more open state of the constriction region indicating that translocation of NH_4^+ from the substrate binding site to the pore lumen is coupled to F107 and F215 side-chain rotations, which supports previous suggestions (9,10).

The hydrophobic pore and the L114 cavity

Fig. 4 *A* shows a vertical cut through the Khademi structure 1U7G and the channel pathway calculated using HOLE (28). The intraluminal channel radii for the Khademi structure and sim-{II,IV,V} are shown in Fig. 4 *B*. The three latter curves represent the smallest (sim-{II,IV}) and largest (sim-V) radii of all conducted simulations. In general, the channel widens relative to the crystal structure. The largest difference is observed around the Am3 position and is due to a conformational change of the L114 side chain, which creates a cavity adjacent to that position. This observation is a general feature, since that region exhibits small deviations in radii when comparing our simulations in Fig. 4 *B*. Larger deviations in radii are observed around the Am2 and Am4 positions. These are due to nonspecific small displacements of M23, V67, I110, H168, W212, and F215, and F31, I28, L114, L208, and I266, respectively. The largest deviations in radii between simulations do, however, not exceed 0.6 Å, which we consider as minor channel radii fluctuations.

A native protonation state of the intraluminal histidines

In general, the intraluminal Amm positions are mutually correlated. The strongest correlation is observed between NH_4^+ and NH_3, but occasionally also between the two NH_3 molecules closest to the periplasm (Fig. 2). These two NH_3 can interchange positions. Interchange may occur when both NH_3 molecules simultaneously occupy the Am3 position and the adjacent L114 cavity, where NH_3 is stabilized by the hydrogen acceptor I110:O. The NH_3 distributions center around the Am3 position (Fig. 4 *B*) and exhibit no significant dependence on the protonation state of the intraluminal Histidines nor on the occupation of the Am2 and/or Am4 positions. This does not apply to NH_3 positioned at the periplasmic or cytoplasmic boundaries, respectively (Fig. 4 *B*).

In sim-IV and sim-V the introduced intraluminal NH_4^+ never occupies the middle of the pore (Fig. 2). This is in accordance with the suggestions of NH_3 being the conducted species and with the barrier against cation conduction being highest in this region (9,10,14).

In the Khademi structure 1U7G, three NH_3 molecules occupy the Am2, Am3, and Am4 positions (Fig. 1 *B*). It is argued that H168:N_ϵH is hydrogen-donor to T273:O_γ, while H318:N_ϵ is hydrogen-acceptor to Amm positioned at Am4 (9), which corresponds to the intraluminal protonation state

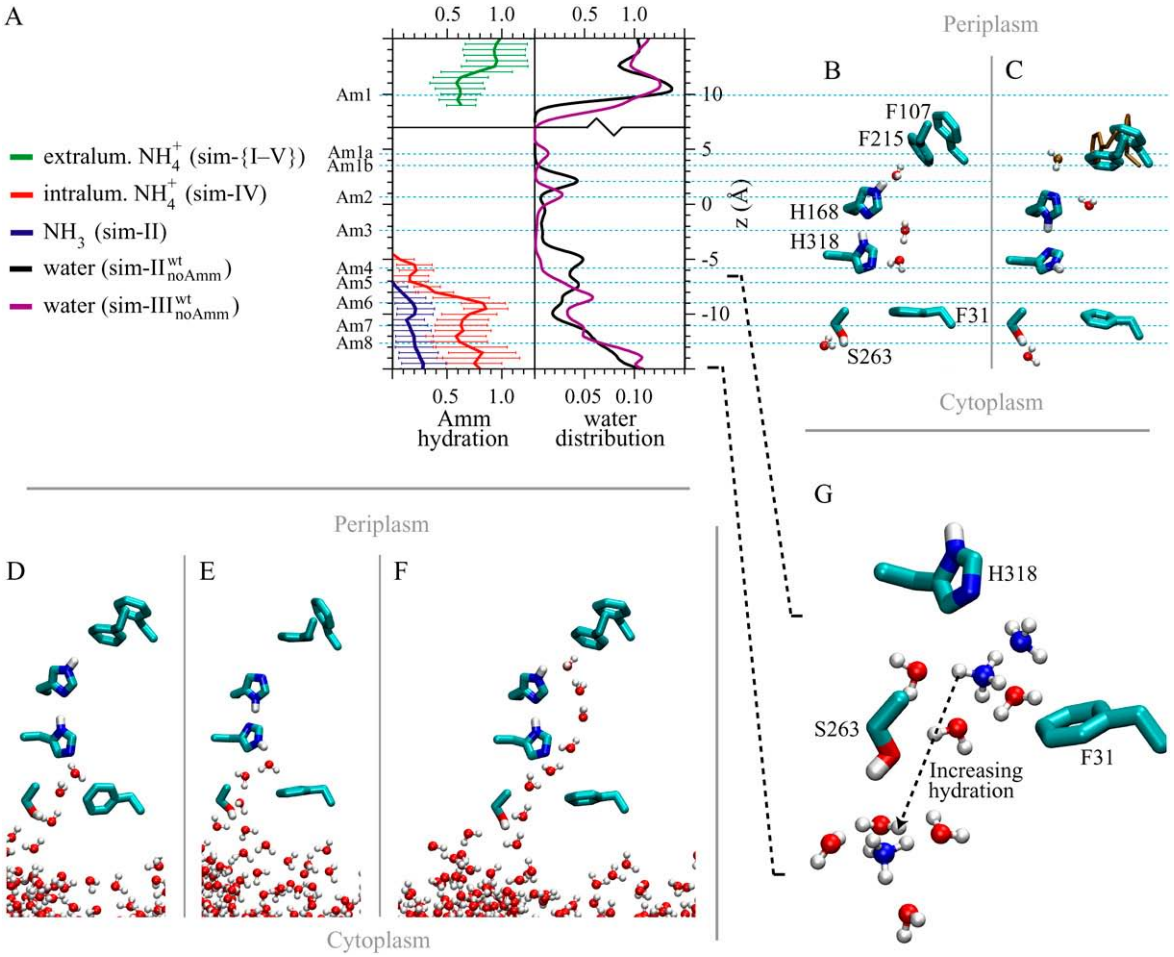

FIGURE 5 Channel hydration. (*A*) The fractional Amm hydration in sim-{I–V} and the distribution of intra- and extraluminal water in sim-II^{wt}_{noAmm} and sim-III^{wt}_{noAmm}. The fractional hydration of Amm was obtained by counting the number of water molecules within 2 Å of Amm during simulations, averaging this number for bins of size 0.5 Å along the *z* direction, and normalizing to the average bulk hydration. Error bars represent the fractional Amm hydration ± SD. The water distribution was obtained by counting the number of water molecules within cylindrical slabs of height 0.1 Å along the *z* direction, and then normalizing by setting bulk water slabs to 1. Due to low water densities in intraluminal slabs the lower graph uses a different scale for the water distribution. Values exceeding 1 arise due to immobilization of water in the periplasmic vestibule (above the substrate binding site Am1) in combination with a small size of the cylindrical slab volume used in our analysis. (*B*) Three water molecules accommodate the pore lumen simultaneously for 1.2 ns in sim-II^{wt}_{noAmm}. (*C*) Maximally, water protrudes up to the Am1a and Am1b positions (*brown*), but cannot stabilize an open state of the F107/F215 stack. Mainly water accommodates the Am2 position, sim-III^{wt}_{noAmm}. (*D*,*E*) Water enters into the pore lumen via single file formation to either H318:N_ϵ or H318:N_ϵH. The single file is stabilized by S263:O_γ(H). (*F*) A single file of water can extend all the way up to the periplasmic constriction region, sim-II^{wt}_{noAmm}. (*G*) NH_4^+ hydration and exit from the pore lumen in sim-IV. NH_4^+ forms a pair with NH_3 and is coordinated to three water molecules. When translocating toward the cytoplasm, NH_4^+ becomes fully coordinated to water and so does NH_3 (not shown). Occasionally, NH_4^+ escape promotes NH_3 escape as well.

of our sim-II (Fig. 1 *D*). However, in this Khademi structure, a β-octylglucoside blocks the cytoplasmic vestibule all the way up to F31, and the aromatic side chain of F31 is slightly lifted upwards relative to the Zheng structures (9,10). When comparing the average positions of intraluminal NH_3 in our simulations, we find that sim-III is in best accordance with the Amm positions found in the Khademi structure 1U7G (Fig. 4 *B*). In sim-III, the most cytoplasmic NH_3 is centered between Am4 and Am5, and conforms to both positions when considering the standard deviations. However, that minor inconsistency with respect to the crystal structure can be explained by the absence of β-octylglucoside in our simulations. Seemingly, presence of the β-octylglucoside shifts the position of the most cytoplasmic NH_3 upward to the Am4 position. Thereby the Khademi structure 1U7G conforms to the idea that the intraluminal protonation state of sim-III is the native state before proton relay. This is supported by our pK_a calculations (see Materials and Methods for details), which yield a larger shift in pK_a (ΔpK_a) for H318:N_ϵ relative to that for H168:N_ϵ, when assuming NH_3 (or water) molecules are occupying the pore lumen. In our simulations, NH_3 and/or water molecules occupy the pore lumen. Thus, we conclude that neutral H168:N_δH-H318:N_ϵH is the native protonation state of H168 and H318 in AmtB.

Hydration and escape of Amm

Fig. 5 *A* shows the average fractional hydration numbers of NH_3 (sim-II) and NH_4^+ (sim-IV) upon escape from the channel lumen. NH_4^+ hydration at an intraluminal position is exceeding that of a correspondingly positioned NH_3. In hydrated form, NH_4^+ leaves the lumen and escapes to the cytoplasmic vestibule (Fig. 5 *G*). Occasionally, a NH_4^+-NH_3 pair is formed (Fig. 5 *G*) and NH_4^+ escape thereby promotes NH_3 escape as well. The first specific interaction observed between NH_4^+ and the cytoplasmic vestibule is to S263:O_γ. Further out the vestibule, specific interactions with the D313 and D309 carboxylate groups also occur. It has been suggested that NH_3 may accept a proton close to the position of the D313 carboxylate group (9). Of note is that this suggestion was based on the 1U7G structure where the cytoplasmic vestibule is blocked by β-octylglucoside. As discussed below, we observe in our simulations that the cytoplasmic vestibule is hydrated up to S263 (Fig. 5, *B–F*). The crystal structures without β-octylglucoside also have water molecules at the Am5–Am8 positions (Fig. 1 *B*), which are closer to the cytoplasmic constriction than D313 (9,10). This suggests that NH_3 is more likely to acquire a proton before reaching the D313 carboxylate group region, probably already when positioned at the Am4–Am5 positions.

We do not observe that Amm escape is correlated with large conformational changes in the N-terminus of TM10 or large V314 displacements as suggested previously (10). Although we cannot rule out long-time protein conformational changes, this seemingly implies that the so-called ''open'' Zheng conformation (1XQE) might not be functionally relevant since the ''closed'' conformation, adopted by all other crystal structures, does not prevent partial Amm conduction according to our results.

Channel hydration and single file water

To investigate channel hydration, we conducted two 10-ns simulations; sim-II^{wt}_{noAmm} and sim-III^{wt}_{noAmm}, with the channel devoid of Amm. The water distribution in Fig. 5 *A* shows that water is present just above the Am1 position and may protrude 2–3 Å below, confirming that the Am1 position is accessible to solvent (9). Fig. 5 *A* also shows that in both simulations water enters the channel lumen, which confirms the suggestion of a partial channel hydration (10), but is at variance with related simulation results (9). We observe that up to three water molecules can occupy the lumen simultaneously and access all positions (Am2–Am5) therein (Fig. 5, *B* and *C*). However, intraluminal water molecules are predominantly positioned at the top and bottom of the channel lumen. The average water positions (Fig. 5 *A*) depend in turn on the protonation state of the two luminal Histidines as exemplified in Fig. 5, *B* and *C*. Interestingly, in both simulations, water entrance occurs by temporary formation of single file water extending from the cytoplasmic vestibule up to H318:N_ϵ and H318:N_ϵH, respectively (Fig. 5, *D* and *E*). Moreover, a single file of water was also observed to form from the cytoplasm and all the way up to the periplasmic constriction region (Fig. 5 *F*). In sim-{I–V} with Amm present in the channel, we observe water entry into the lumen also solely from cytoplasm. In all cases, S263:O_γ promotes formation of single file water inside the channel (Fig. 5, *D–F*).

Single file water can conduct protons (29). Even if water-mediated proton conduction through the hydrophobic environment in the middle of the channel lumen is energetically unfavorable (10), at least proton conduction between cytoplasm and H318:N_ϵ is possible. Thus, proton conduction by single-file water provides a possible mechanism for H^+ exchange with H168/H318.

No water crossing of the periplasmic hydrophobic constriction was observed in any simulation in accordance with the fact that AmtB does not sustain water transport (9). Experiments also show that the channel does not conduct cations other than Amm and MeAmm. Water and cation filtering mechanisms are discussed below.

Mechanisms

To prevent leakage of water and cations, a two-filter system presumably has to be present in AmtB; one filter that excludes water, and one that excludes cations other than NH_4^+ or $MeNH_3^+$ from passing through.

Water filtering at the F107/F215 stack

Our simulations indicate that specifically the periplasmic hydrophobic constriction is impermeable to water. Transfer of any substrate across the constriction region presupposes rotation of F107 and F215 (Figs. 3 *C* and 5 *C*). We observe that NH_4^+ can induce and stabilize a transient open state of the F107/F215 stack for several nanoseconds (Fig. 3 *C*), while neither NH_3 or water can (Fig. 5 *C*). Thus, we propose that the F107/F215 stack and the otherwise hydrophobic character of the constriction region constitutes a filter against water transport.

Cation filtering at intraluminal NH_4^+ binding sites

A water filter should also filter NH_3, a hydrogen donor/acceptor and polar molecule like water. Combined with the observed stabilization of the F107/F215 stack mentioned above, this suggests that NH_4^+ is the Amm species transported across the constriction region. This is supported by free energy calculations, which identified cationic binding sites on both the extra- and intraluminal sides (10). A cation filtering function of the constriction region was also suggested, but only selectivity against Na^+ ions, while not against K^+ ions, could be explained (10). We have identified two intraluminal binding sites both providing tetrahedral

coordination of NH_4^+. In other ion channels, binding sites selective of Na^+ require 5–6 coordinating oxygens, while those selective of K^+ require eight coordinating oxygens and a larger binding cavity due to its larger size ((30), and references therein). Since NH_4^+ is roughly the same size as K^+, one may speculate that AmtB, due to the size of its intraluminal binding cavities (i.e., it accommodates both NH_4^+ and the larger $MeNH_3^+$), cannot coordinate Na^+ efficiently, as observed for other selectivity filters ((30), and references therein). The coordination provided by AmtB probably cannot stabilize K^+ either. Thus, we speculate that the tetrahedral coordination in AmtB is selective of NH_4^+, i.e., it counterbalances the dehydration cost of NH_4^+ better than that of other cations. In conjunction with the hydrophobic pore lumen, which prevents cation transfer (9,10), this provides an intriguing cation filter mechanism. We do not hereby exclude that the F107/F215 stack may also provide some discrimination among cations.

Luminal ammonium binding and proton transfer

Since the recruited Amm species is NH_4^+, while the transported Amm species is NH_3, proton transfer reactions must occur at the channel entrance. According to our discussion above, deprotonation of NH_4^+ takes place after NH_4^+ transfer across the F107/F215 stack and before further translocation down the pore. As previously argued, the protonation state of luminal Histidines before proton relay is assumed to be the neutral H168:N_δH-H318:N_ϵH state. Since AmtB has been shown not to conduct protons (9), a proton must be transferred back to the periplasm. This proton transfer can be mediated by A162:C=O as shown in Fig. 6, which in our simulations forms a conserved H-bond with NH_4^+ when it is bound in the periplasmic constriction region. First A162:C=O guides NH_4^+ across the F107/F215 stack (Fig. 6, step *1*). When NH_4^+ occupies the Am1a or Am1b positions, we find that a perfectly aligned H-bond can be established between the backbone NH of the A162-G163 peptide bond and D160:O_δ (Fig. 6, step *2*). In general, hydrogen exchange of NH can be catalyzed by a base, i.e., deprotonation of NH, or by an acid, i.e., protonation of either O or N. The O protonation, the so-called imidic acid mechanism, is preferred in proteins (31,32). In our case, both intraluminal NH_4^+ and partially solvent-accessible D160:O_δ may be considered as a stronger acid and a stronger base, respectively, when compared to their solvated counterparts. Thus, they can catalyze the hydrogen exchange via the imidic acid mechanism as a combination of base and acid catalysis (Fig. 6, step *2*). When the proton is effectively transferred from NH_4^+ to D160:O_δ it yields an intermediate state where all involved parts are neutral and A162:C-O-H reorients to the substrate binding site (Fig. 6, step *3*). The reorientation and thereby a less favorable interaction between G163:N and D160:O_δ-H, due to a changed direction of the H-bond, both promote proton

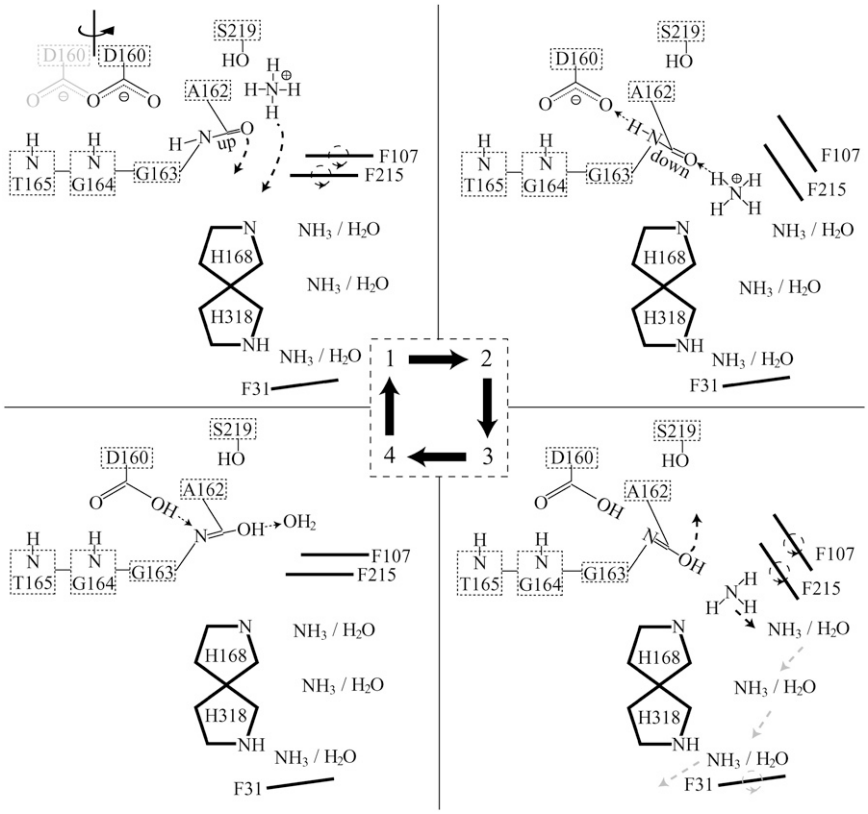

FIGURE 6 Proton transfer mechanism. (*1*) At the substrate binding site NH_4^+ H-bonds to S219:O_γ and A162:C=O. D160 can interact with NH_4^+ and G163:NH by rotation of its carboxylate group. In correlation with F107 and F215 rotation, NH_4^+ translocates to the channel lumen guided by A162:C=O. (*2*) When A162:C=O points into the lumen, G163:NH aligns to form a H-bond with D160:O_δ. Hydrogen exchange at the A162-G163 peptide bond is then catalyzed by D160 and NH_4^+, resulting in a net proton transfer from NH_4^+ to D160:O_δ, thereby yielding an imidic acid intermediate. (*3*) Charges on D160 and NH_4^+ are neutralized. NH_3 translocates further down the lumen. At some point the A162-G163 peptide bond reorients to the substrate binding site. Translocation of NH_3 may occur in any step and the gray arrows merely indicate one of several possible translocation mechanisms. (*4*) At an intermediate step between step *3* and step *1*, the imidic acid mechanism is reversed due to a less favorable H-bond between D160:O_δH and G163:N, and a proton is transferred to water thereby recovering the initial state.

transfer to a periplasmic water molecule to recover the initial state (Fig. 6, step *4*). This proposed proton transfer mechanism also adds a new explanation to the experiment where Amm conduction is lost upon D160 mutation, e.g., D160A; only the D160E mutation retains function (25). Additionally, we have observed that rotation of the D160 carboxylate group may occur when NH_4^+ is bound at the substrate binding site. This provides an appealing coupling between NH_4^+ recruitment and the proton transfer mechanism described above. Our simulations do not provide information about the translocation mechanism of Amm further down the pore lumen. In Fig. 6 (step *3*) only one of several possible translocation mechanisms of intraluminal NH_3 is indicated. However, a mechanism that couples NH_4^+ entrance to the escape/protonation of an Am4-Am5 positioned NH_3, via the H168-H318 ring system, is also alluring.

CONCLUSION

We have conducted molecular dynamics simulations of *E. coli* AmtB with different protonation states of intraluminal H168, H318, and Amm. Additional simulations were conducted to investigate channel hydration and whether the differing configurations of substrate binding site residues in the x-ray structures affect substrate binding. Our simulations show that the Q104 side chain does not affect recruitment and binding of NH_4^+ to the substrate binding site, but that it may affect recruitment and binding of other substrates, e.g., MeAmm. We identified novel NH_4^+-protein interactions involved in NH_4^+ recruitment, whereof interactions with D160:O_δ and A162:C=O are of special interest. Our simulations indicate that D160 not only has a structural function, but is also directly involved in NH_4^+ binding at the substrate binding site. A162:C=O was observed to reorient to coordinate NH_4^+ when positioned either intraluminally or extraluminally. This suggests that the function of A162:C=O is to guide NH_4^+ across the F107/F215 stack. In addition, we suggest that hydrogen exchange at the A162-G163 peptide bond via the imidic acid mechanism, plausible as catalyzed by the D160 carboxylate group and intraluminal NH_4^+, provides a mechanism for transferring a proton from intraluminal NH_4^+ to a periplasmic water molecule. Thus D160 is a prerequisite for conduction.

We have identified two intraluminal binding sites, Am1a and Am1b, both providing tetrahedral coordination of NH_4^+, which again stabilizes transient open states of the F107/F215 stack. This indicates that NH_4^+ may translocate from the substrate binding site to intraluminal positions before its deprotonation. Based on our observations and conducted pK_a calculations, we conclude that the protonation state of luminal Histidines before any proton relay is H168:N_δH-H318:N_ϵH. In addition, we propose that the intraluminal binding sites are selective of NH_4^+ over other cations such as K^+ and Na^+, which require different coordination numbers, and thus represent a cation filter. We do not observe intraluminal NH_4^+ translocation across the middle of the pore lumen, which supports the view of NH_3 being the conducted species.

Water is able to enter the channel from cytoplasm via single file formation to H318:N_ϵ(H). Occasionally, a single file can be supported all the way up through the channel lumen. We have implied that our observation of luminal water and single file water may provide a means of proton transfer between H168, H318 and Amm, as well as between lumen and cytoplasm. We do not observe water crossing the periplasmic hydrophobic constriction region. Therefore, we suggest that the F107/F215 stack and the otherwise hydrophobic character of the constriction region constitute a filter against water transport.

The authors thank Flemming Y. Hansen, Ask F. Jakobsen, and Jacob Sonne for valuable discussions.

The authors acknowledge financial support by the Danish National Research Foundation via a grant to the MEMPHYS - Center for Biomembrane Physics, and computing time provided at the Danish Center for Scientific Computing at the University of Southern Denmark, Odense. T.P.N and M.O.J. acknowledge a travel grant from HCP-Europa. The molecular images in this article were created with Visual Molecular Dynamics (16).

REFERENCES

1. Transport Classification Database (TCDB). 2005. http://www.tcdb.org/.
2. Murzin, A. G., S. E. Brenner, T. Hubbard, and C. Chothia. 1995. SCOP: a structural classification of proteins database for the investigation of sequences and structures. *J. Mol. Biol.* 247:536–540.
3. Kleiner, D. 1993. NH_4^+ transport systems. *In* Alkali Cation Transport Systems in Prokaryotes. E. P. Bakker, editor. CRC Press, Boca Raton, FL. 379–396.
4. Hackette, S. L., G. E. Skye, C. Burton, and I. H. Segel. 1970. Characterization of an ammonium transport system in filamentous fungi with methylammonium-14C as the substrate. *J. Biol. Chem.* 245: 4241–4250.
5. Siewe, R. M., B. Weil, A. Burkovski, B. J. Eikmanns, M. Eikmanns, and R. Krämer. 1996. Functional and genetic characterization of the (methyl)ammonium uptake carrier of *Corynebacterium glutamicum*. *J. Biol. Chem.* 271:5398–5403.
6. Soupene, E., L. He, D. Yan, and S. Kustu. 1998. Ammonia acquisition in enteric bacteria: physiological role of the ammonium/methylammonium transport B (AmtB) protein. *Proc. Natl. Acad. Sci. USA.* 95: 7030–7034.
7. Marini, A.-M., G. Matassi, V. Raynal, B. Andre, J.-P. Cartron, and B. Cherif-Zahar. 2000. Letters—the human Rhesus-associated RhAG protein and a kidney homologue promote ammonium transport in yeast. *Nat. Genet.* 26:341–344.
8. Soupene, E., N. King, E. Feild, P. Liu, K. K. Niyogi, C.-H. Huang, and S. Kustu. 2002. Biological sciences-physiology-rhesus expression in a green alga is regulated by CO_2. *Proc. Natl. Acad. Sci. USA.* 99:7769–7773.
9. Khademi, S., J. O'Connell, J. Remis, Y. Robles-Colmenares, L. J. W. Miercke, and R. M. Stroud. 2004. Mechanism of ammonia transport by Amt/MEP/Rh: structure of AmtB at 1.35 Å. *Science.* 305:1587–1594.
10. Zheng, L., D. Kostrewa, S. Berneche, F. K. Winkler, and X. D. Li. 2004. The mechanism of ammonia transport based on the crystal structure of AmtB of *Escherichia coli*. *Proc. Natl. Acad. Sci. USA.* 101: 17090–17095.
11. Blakey, D., A. Leech, G. H. Thomas, G. Coutts, K. Findlay, and M. Merrick. 2002. Research papers—purification of the *Escherichia coli* ammonium transporter AmtB reveals a trimeric stoichiometry. *Biochem. J.* 364:527–536.

12. Conroy, M. J., S. J. Jamieson, D. Blakey, T. Kaufmann, A. Engel, D. Fotiadis, M. Merrick, and P. A. Bullough. 2004. Electron and atomic force microscopy of the trimeric ammonium transporter AmtB. *EMBO Rep*. 5:1153–1158.

13. Liu, Y., and X. Hu. 2006. Molecular determinants for binding of ammonium ion in the ammonia transporter AmtB–a quantum chemical analysis. *J. Phys. Chem. A Mol. Spectrosc. Kinet. Environ. Gen. Theory*. 110:1375–1381.

14. Javelle, A., G. Thomas, A.-M. Marini, R. Kramer, and M. Merrick. 2005. In vivo functional characterization of the *Escherichia coli* ammonium channel AmtB: evidence for metabolic coupling of AmtB to glutamine synthetase. *Biochem. J*. 390:215–222.

15. Kale, L., R. Skeel, M. Bhandarkar, R. Brunner, A. Gursoy, N. Krawetz, J. Phillips, A. Shinozaki, K. Varadarajan, and K. Schulten. 1999. NAMD2: greater scalability for parallel molecular dynamics. *J. Comput. Phys*. 151:283–312.

16. Humphrey, W., A. Dalke, and K. Schulten. 1996. VMD: visual molecular dynamics. *J. Mol. Graph*. 14:33–38.

17. Tieleman, D. P., and H. J. C. Berendsen. 1998. A molecular dynamics study of the pores formed by *Escherichia coli* OmpF porin in a fully hydrated palmitoyloleoylphosphatidylcholine bilayer. *Biophys. J*. 74: 2786–2801.

18. Rappolt, M., A. Hickel, R. Bringezu, and K. Lohner. 2003. Mechanism of the lamellar/inverse hexagonal phase transition examined by high resolution x-ray diffraction. *Biophys. J*. 84:3111–3122.

19. Grubmüller, H. 1996. SOLVATE v1.0. Theoretical Biophysics Group, Institut für Medizinische Optik, Ludwig-Maximilians-Universität München, München, Germany.

20. MacKerell Jr., A. D., D. Bashford, M. Bellott, R. L. Dunbrack Jr., J. D. Evanseck, M. J. Field, S. Fischer, J. Gao, H. Guo, S. Ha, D. Joseph-McCarthy, L. Kuchnir, K. Kuczera, F. T. K. Lau, C. Mattos, S. Michnick, T. Ngo, D. T. Nguyen, B. Prodhom, W. E. Reiher III, B. Roux, M. Schlenkrich, J. C. Smith, R. Stote, J. Straub, M. Watanabe, J. Wiorkiewicz-Kuczera, D. Yin, and M. Karplus. 1998. All-atom empirical potential for molecular modeling and dynamics studies of proteins. *J. Phys. Chem. B*. 102:3586–3616.

21. Chen, I. J., D. Yin, and A. D. MacKerell, Jr. 2002. Combined ab initio/empirical approach for optimization of Lennard-Jones parameters for polar-neutral compounds. *J. Comput. Chem*. 23:199–213.

22. Jorgensen, W. L., and J. Gao. 1986. Monte Carlo simulations of the hydration of ammonium and carboxylate ions. *J. Phys. Chem.* 90:2174–2182.

23. Faraldo-Gomez, J. D., and B. Roux. 2004. Electrostatics of ion stabilization in a ClC chloride channel homologue from *Escherichia coli*. *J. Mol. Biol*. 339:981–1000.

24. Brooks, B. R., R. E. Bruccoleri, B. D. Olafson, D. J. States, S. Swaminathan, and M. Karplus. 1983. CHARMM: a program for macromolecular energy, minimization, and dynamics calculations. *J. Comput. Chem*. 4:187–217.

25. Javelle, A., E. Severi, J. Thornton, and M. Merrick. 2004. Ammonium sensing in *Escherichia coli*: role of the ammonium transporter AmtB and AmtB-GlnK complex formation. *J. Biol. Chem*. 279:8530–8538.

26. Kaback, H. R. 2005. Structure and mechanism of the lactose permease. *C. R. Biol*. 328:557–567.

27. Karim, O. A., and A. D. J. Haymet. 1990. Dynamics of an ammonium ion in water: molecular-dynamics simulation. *J. Chem. Phys*. 93:5961–5966.

28. Smart, O. S., J. M. Goodfellow, and B. A. Wallace. 1993. The pore dimensions of gramicidin. *Biophys. J*. 65:2455–2460.

29. Agmon, N. 1995. The Grotthuss mechanism. *Chem. Phys. Lett*. 224:456–462.

30. Gouaux, E., and R. MacKinnon. 2005. Principles of selective ion transport in channels and pumps. *Science*. 310:1461–1465.

31. Perrin, C. L. 1989. Proton exchange in amides: surprises from simple systems. *Acc. Chem. Res*. 22:268–275.

32. Dempsey, C. E. 2001. Hydrogen exchange in peptides and proteins using NMR spectroscopy. *Prog. Nucl. Magn. Reson. Spectrosc*. 39:135–170.